Design of Preview Controller for Aviation Electric Fuel Pump Based on Adaptive Sliding Mode Feedback Linearization

MENG Xiangshuo[1], *XIAO Lingfei*[1,2*], *MA Leiming*[3]

1. College of Energy and Power Engineering, Nanjing University of Aeronautics and Astronautics, Nanjing 210016, P. R. China;
2. State Key Laboratory of Fluid Power and Mechatronic Systems, Zhejiang University, Hangzhou 310027, P. R. China;
3. College of Automation Engineering, Nanjing University of Aeronautics and Astronautics, Nanjing 211106, P. R. China

(Received 15 October 2021; revised 10 June 2022; accepted 17 September 2022)

Abstract: This study takes an aviation electric fuel pump with an external gear pump directly driven by a six-phase permanent magnet synchronous motor as an object. Its fuel flow control system is studied in this paper, and a preview controller design approach based on adaptive sliding mode feedback linearization is proposed. Firstly, the mathematical model of six-phase permanent magnet synchronous motor and external gear pump is established. Secondly, the nonlinear model of the electric fuel pump is processed using the feedback linearization method, which is helpful for the following preview controller design. Then, the linearization errors caused by the model uncertainty are eliminated using an adaptive sliding mode control method, which can separate the uncertainty brought on by modeling error and load disturbance and prevent chattering brought on by high switching gain. At the same time, it does not require accurate uncertainty boundary information, which improves control performance. Finally, the linearization model created by the feedback linearization method is used to construct the preview controller, which will reduce the time the control system takes to respond to a fuel command. The simulation results demonstrate that the proposed control method has a less response time, strong robustness, and excellent chattering suppression ability.

Key words: aviation electric fuel pump; preview control; adaptive sliding mode control; feedback linearization; modeling uncertainty

CLC number: V233.7 **Document code:** A **Article ID:** 1005-1120(2023)01-0047-13

0 Introduction

As the core subsystem of more electric aircraft, more electric engine aims to replace parts of traditional hydraulic, pneumatic, and mechanical systems with electricity[1-2], the structure and performance of the engine can be comprehensively optimized. Compared with the traditional aero-engine, the main technical features of the more electric engine include high-power integral starter/engine, active maglev bearing system, distributed control system, electric actuator, and electric fuel pump[3-5]. Among them, the electric fuel pump is the main element of more electric engines since it serves as the supply device in the fuel system of more electric aircraft.

A fixed displacement gear pump powered by an accessory casing serves as the fuel pump in traditional aero engines, which means its speed is directly related to the engine. In some conditions, the fuel provided by the gear pump is much higher than that required by the engine, so additional pipelines need to be added for cooling and reflux of the excess fuel, increasing the complexity of the system[6]. The electric fuel pump composed of motor and gear pump has an independent controller[7], which can adjust the motor speed according to the fuel commands to provide the fuel required by the engine, without cooling and refluxing pipes, thus reducing the

*Corresponding author, E-mail address: lfxiao@nuaa.edu.cn.

How to cite this article: MENG Xiangshuo, XIAO Lingfei, MA Leiming. Design of preview controller for aviation electric fuel pump based on adaptive sliding mode feedback linearization[J]. Transactions of Nanjing University of Aeronautics and Astronautics, 2023, 40(1): 47-59.

http://dx.doi.org/10.16356/j.1005-1120.2023.01.005

weight of the system.

However, the motor in the electric fuel pump usually has large inertia, whether the response speed of the fuel pump to the fuel command can meet the requirement of the engine is a problem worth paying attention to. At the same time, for electric fuel pump, a research object with complex characteristics, an accurate mathematical model is difficult to obtain, and modeling errors often exist in the modeling process. Furthermore, the engine's high temperature, high pressure, and high vibration environment may have an impact on the motor parameters. A key issue that researchers are looking into is how to ensure that the electric fuel pump can supply fuel on demand for aero engines quickly and accurately while taking into account many unknown factors[8].

A control method known as preview control[9] makes full advantage of the system's known future information. It is possible to create a controller with an information compensation feature to significantly increase the system tracking accuracy and shorten response time. The effective combination of preview control and modern control methods is the research focus of preview control theory, and some of the achievements are gradually applied in the aerospace field. In Ref.[10], the spacecraft engine modes were precisely transitioned in different flight phases using the segmented robust preview control method. To compensate for the tracking performance degradation caused by the pilot input delay and the aircraft uncertainty, Ref.[11] introduced preview control to assist driving, effectively overcoming the problem of driver's operation delay. Based on the linear variable parameter model of the aircraft, preview control was introduced based on gain scheduling control in Ref.[12], which effectively reduced the vertical acceleration of the aircraft under gust conditions. In Ref.[13], the glide track of carrier-borne aircraft was taken as previewable information, and the deck fluctuation is compensated by the preview control, to achieve a safe and stable landing of carrier-borne aircraft. When the aircraft is in an automatic driving state, the fuel flow required by the engine can be obtained according to the predetermined attitude, heading, altitude, and Mach number, etc. Then preview control is implemented, and the electric fuel pump's response time to fuel commands can be accelerated by utilizing the information already known about fuel flow.

Sliding mode control has become a popular special nonlinear control strategy due to its quick response and robustness to external disturbances and system parameter changes. However, the robustness of sliding mode control comes at the cost of high-frequency chattering of the controlled variable. For high-precision servo systems such as electric fuel pump, reducing the sliding mode control's chattering problem is essential because the high-frequency of the controlled variable chattering may damage the motor and decrease control performance. In summary, the research is mainly carried out from the aspects of reaching law, switching function, filtering, and disturbance observer. Ref.[14] established the reaching law based on the high-order disturbance compensator and the dead zone function, and while obtaining the quasi-sliding mode of the boundary layer with adjustable order, the chattering is further reduced. In Ref.[15] a non-smooth term was introduced to replace the traditional method of switching items and it achieved higher control accuracy while reducing chattering. Ref.[16] introduced a sliding mode low-pass filter depending on conventional sliding mode control to reduce the chattering problem of sliding mode control. In Ref.[17], the disturbance was evaluated and compensated for using the radial basis function neural network, which weakened the chattering problem of sliding mode control.

This paper provides an adaptive sliding mode feedback linearization-based design approach for a preview controller with the characteristics of quick response speed and high robustness requirements for the aviation electric fuel pump flow control system. Firstly, a model of an external gear pump directly driven by a six-phase permanent magnet synchronous motor (PMSM) is established. Secondly, the linear model after feedback linearization is used to construct the preview controller, improving the response speed of control system to the fuel command. Finally, the linearization error caused by

modeling error and load disturbance is eliminated by using the adaptive sliding mode control method, and the reachability of the sliding mode surface is demonstrated theoretically, as well as the stability of the closed-loop system.

1 Aviation Electric Fuel Pump Model

Since the multiphase PMSM has a high efficiency, a small volume, and reliable operation, and the external gear pump has a lightweight, good self-priming performance, and a simple structure, this paper adopts the electric fuel pump structure of an external gear pump directly driven by a six-phase PMSM.

1.1 Model of the six-phase PMSM

Using the coordinate transformation method of vector space decoupling[18], the current equation of the surface-mounted six-phase PMSM under d-q subspace is

$$\begin{cases} \dfrac{\mathrm{d}}{\mathrm{d}t} i_d = -\dfrac{R}{L} i_d + p\omega_{\mathrm{m}} i_q + \dfrac{1}{L} u_d \\ \dfrac{\mathrm{d}}{\mathrm{d}t} i_q = -\dfrac{R}{L} i_q - p\omega_{\mathrm{m}} i_d - \dfrac{p\psi_{\mathrm{f}}}{L} \omega_{\mathrm{m}} + \dfrac{1}{L} u_q \end{cases} \tag{1}$$

where u_d and u_q are the d-q axis quantity of stator voltage; i_d and i_q the d-q axis quantity of stator current; and R and L the stator resistance and stator inductance, respectively. p is the number of pole-pairs; ω_{m} the mechanical angular velocity of the motor; and ψ_{f} the permanent magnet flux linkage.

Without considering the load torque, the mechanical motion equation of the PMSM is

$$J \frac{\mathrm{d}\omega_{\mathrm{m}}}{\mathrm{d}t} = 3p\psi_{\mathrm{f}} i_q - B\omega_{\mathrm{m}} \tag{2}$$

where J is the rotational inertia, and B the damping coefficient.

The current equation under x-y subspace can be shown as

$$\begin{cases} \dfrac{\mathrm{d}}{\mathrm{d}t} i_x = -\dfrac{R}{L_z} i_x + \dfrac{1}{L_z} u_x \\ \dfrac{\mathrm{d}}{\mathrm{d}t} i_y = -\dfrac{R}{L_z} i_y + \dfrac{1}{L_z} u_y \end{cases} \tag{3}$$

where u_x and u_y are the x-y axis quantity of stator voltage; i_x and i_y the x-y axis quantity of stator current; and L_z is the stator leakage sensation.

Since the current in the x-y subspace has no contribution to the generation of electromagnetic torque, it will only increase the stator copper loss, so the desired value is usually set to zero, and only the stator current components in the d-q subspace are considered, to ensure the maximum torque output and minimum copper loss of the motor.

We set the state vector $\boldsymbol{x} = [\, i_d \quad i_q \quad \omega_{\mathrm{m}} \,]^{\mathrm{T}}$, the input vector $\boldsymbol{u} = [\, u_d \quad u_q \,]^{\mathrm{T}}$, and define the output vector

$$\begin{cases} y_1 = h_1(\boldsymbol{x}) = i_d \\ y_2 = h_2(\boldsymbol{x}) = \omega_{\mathrm{m}} \end{cases} \tag{4}$$

The standard affine nonlinear equation of system Eq.(1) and system Eq.(2) can be obtained

$$\begin{cases} \dot{\boldsymbol{x}} = \boldsymbol{f}(\boldsymbol{x}) + \boldsymbol{g}(\boldsymbol{x})\boldsymbol{u} \\ \boldsymbol{y} = \boldsymbol{h}(\boldsymbol{x}) \end{cases} \tag{5}$$

where $\boldsymbol{f}(\boldsymbol{x}) = \begin{bmatrix} -Ri_d/L + p\omega_{\mathrm{m}} i_q \\ -Ri_q/L - p\omega_{\mathrm{m}} i_d - p\psi_{\mathrm{f}}\omega_{\mathrm{m}}/L \\ 3p\psi_{\mathrm{f}} i_q/J - B\omega_{\mathrm{m}}/J \end{bmatrix}$, and $\boldsymbol{g}(\boldsymbol{x}) = \begin{bmatrix} 1/L & 0 \\ 0 & 1/L \\ 0 & 0 \end{bmatrix}$.

1.2 Model of the external gear pump

A gear pump operates by enlarging the oil suction cavity and compressing the oil discharge cavity to absorb and discharge oil. For a gear pump with two identical gears and an ideal unloading groove, its instantaneous flow is[19]

$$q_v(t) = B\omega\left(R_{\mathrm{a}}^2 - R_{\mathrm{c}}^2 - R_{\mathrm{b}}^2\varphi\right) \tag{6}$$

where B is the tooth width of the gear, ω the angular velocity of the gear, R_{a} the radius of the addendum circle, R_{c} the radius of the pitch circle, R_{b} the radius of the base circle, and φ the rotation angle of the gear.

The instantaneous flow of the gear pump exhibits a parabolic change with the gear rotation angle, as can be observed from Eq.(6).

During the process of meshing and discharging the oil, the meshing point moves back and forth at a fixed interval along the meshing line. The fuel volume V_n discharged by a pair of meshing gear teeth during a cycle corresponds to the meshing point passing through a complete base pitch P_{b}, so as to get the theoretical output flow of the fuel pump

$$Q_t = \omega z \int_{P_b} q_v(t)\,\mathrm{d}t = 2\pi n B\left(R_a^2 - R_c^2 - \frac{P_b^2}{12}\right) \quad (7)$$

where z is the tooth number of the gear, and n the rotational speed of the gear.

In addition, considering the leakage flow at the end face, radial clearance, and meshing point, there will also be some elastic loss when the liquid is compressed. At the same time, when the clearance value is certain, the leakage flow increases as the pressure differential between the gear pump's input and outlet increases. Therefore, it is challenging to create an accurate model of leakage flow. A throttling orifice[20], in which the internal pressure is the outlet pressure of gear pump oil and the back pressure is the inlet pressure of gear pump oil, is utilized to imitate the leakage flow.

$$Q_l = C_d A_t \sqrt{\frac{2(P_o - P_i)}{\rho}} \quad (8)$$

where C_d is the throttling coefficient, A_t the throttling orifice area, P_o the oil outlet pressure, P_i the oil inlet pressure, and ρ the fuel density.

As a result, the actual output flow of gear pump is

$$Q = Q_t - Q_l \quad (9)$$

Refer to the leakage flow calculation method, the actual flow of the gear pump can also be determined by the oil outlet, in which the internal pressure of the oil outlet is the oil outlet pressure of the gear pump, and the back pressure is the pressure of the fuel tank.

$$Q = C_d A_o \sqrt{\frac{2(P_o - P_t)}{\rho}} \quad (10)$$

where A_o is the oil outlet area, and P_t the fuel tank pressure.

Therefore, considering the leakage flow, the relationship between the actual flow and the gear speed can be determined according to Eqs.(7—9), shown as

$$n = \frac{Q + C_d A_t \sqrt{2(P_o - P_i)/\rho}}{2\pi B\left(R_a^2 - R_c^2 - P_b^2/12\right)} \quad (11)$$

where the oil outlet pressure P_o can be obtained according to Eq.(10), shown as

$$P_o = P_t + \frac{\rho Q^2}{2C_d^2 A_o^2} \quad (12)$$

The radial forces produced by hydraulic pressure and gear meshing make up the majority of the radial forces produced by the gear pump. Among these, the motor is directly impacted by the torque created by gear meshing, and the specific calculation formula is[21]

$$T_L = \frac{(P_o - P_i) B R_b^2}{2}\left[\frac{\left(\tan^2\alpha_a - \tan^2\alpha'\right)}{\eta_1} + \frac{\left(\tan^2\alpha_a - \tan^2\alpha\right)}{\eta_1\eta_2}\right] \quad (13)$$

where α_a is the pressure angle of the addendum circle. α and α' are the pressure angles at the meshing points of the driving gear and the driven gear; η_1 and η_2 the mechanical efficiency of the driving gear and the driven gear.

According to Eq.(7), it can be seen that for an external gear pump whose size parameters are determined, its theoretical flow is only related to the speed of the gear. Therefore, the fuel flow command can be converted into a speed command by Eq.(11), the flow of the gear pump can be regulated indirectly by adjusting the PMSM rotational speed, and the gear pump is regarded as a load of the PMSM.

2 Design of Preview Controller Based on Adaptive Sliding Mode Feedback Linearization

It can be seen from the above analysis that the electric fuel pump is a strongly coupled nonlinear system, which significantly enhances the challenge of designing the preview controller. Thus, a feedback linearization technique is first utilized to deal with the nonlinear model of the six-phase PMSM, and then an adaptive sliding mode method is utilized to remove the influence of uncertainty produced by modeling error and the gear pump load disturbance. Based on the linear model, the preview controller is designed finally.

2.1 Feedback linearization method based on adaptive sliding mode controller

2.1.1 Feedback linearization of the six-phase PMSM

According to Eq.(5), it is clear that the six-

phase PMSM model is a typical nonlinear and strong coupling system. To achieve complete decoupling and facilitate the design of preview controller, feedback linearization[22] is adopted for linear processing.

The Lie derivatives of the output vectors i_d and ω_m the system are obtained

$$\begin{cases} L_f h_1(\boldsymbol{x}) = -Ri_d/L + p\omega_m i_q \\ L_{g1} h_1(\boldsymbol{x}) = 1/L \\ L_f h_2(\boldsymbol{x}) = 3p\psi_f i_q/J - B\omega_m/J \\ L_{g2} h_2(\boldsymbol{x}) = 0 \\ L_f^2 h_2(\boldsymbol{x}) = -\left(3p\psi_f R/JL + 3p\psi_f B/J^2\right) i_q + \\ \qquad \left(B^2/J^2 - 3p^2\psi_f^2/JL\right)\omega_m - 3p^2\psi_f\omega_m i_d/J \\ L_{g1} L_f h_2(\boldsymbol{x}) = 0 \\ L_{g2} L_f h_2(\boldsymbol{x}) = 3p\psi_f/JL \end{cases} \tag{14}$$

Then Eq.(5) can be written as

$$\begin{bmatrix} \dot{i}_d \\ \ddot{\omega}_m \end{bmatrix} = \begin{bmatrix} L_f h_1(\boldsymbol{x}) \\ L_f^2 h_2(\boldsymbol{x}) \end{bmatrix} + \begin{bmatrix} L_{g1} h_1(\boldsymbol{x}) & L_{g2} h_1(\boldsymbol{x}) \\ L_{g1} L_f h_2(\boldsymbol{x}) & L_{g2} L_f h_2(\boldsymbol{x}) \end{bmatrix} \boldsymbol{u} = F(\boldsymbol{x}) + G(\boldsymbol{x})\boldsymbol{u} \tag{15}$$

Through differential homeomorphism transformation

$$\begin{cases} z_1 = h_1(\boldsymbol{x}) = i_d \\ z_2 = h_2(\boldsymbol{x}) = \omega_m \\ z_3 = L_f h_2(\boldsymbol{x}) = 3p\psi_f i_q/J - B\omega_m/J \end{cases} \tag{16}$$

the virtual input vector $\boldsymbol{v}$ is defined as

$$\begin{cases} \dot{z}_1 = \dot{y}_1 = v_1 \\ \dot{z}_2 = z_3 \\ \dot{z}_3 = \ddot{y}_2 = v_2 \end{cases} \tag{17}$$

And the linear system model of the six-phase PMSM is obtained as

$$\begin{cases} \dot{\boldsymbol{z}} = \boldsymbol{A}\boldsymbol{z} + \boldsymbol{B}\boldsymbol{v} = \begin{bmatrix} 0 & 0 & 0 \\ 0 & 0 & 1 \\ 0 & 0 & 0 \end{bmatrix} \boldsymbol{z} + \begin{bmatrix} 1 & 0 \\ 0 & 0 \\ 0 & 1 \end{bmatrix} \boldsymbol{v} \\ \boldsymbol{y} = \boldsymbol{C}\boldsymbol{z} = \begin{bmatrix} 1 & 0 & 0 \\ 0 & 1 & 0 \end{bmatrix} \boldsymbol{z} \end{cases} \tag{18}$$

The nominal linear system is used as a reference model

$$\begin{bmatrix} \dot{y}_{m1} \\ \ddot{y}_{m2} \end{bmatrix} = F(\boldsymbol{x}) + G(\boldsymbol{x})\boldsymbol{u} \tag{23}$$

Then the linearization error of the system Eq.(22) is defined as

$$\boldsymbol{e}_m = \begin{bmatrix} e_{m1} \\ e_{m2} \end{bmatrix} = \begin{bmatrix} y_1 - y_{m1} \\ y_2 - y_{m2} \end{bmatrix} \tag{24}$$

The current subsystem is a first-order system, and the speed subsystem is a second-order system,

The input of system Eq.(5) can be obtained through nonlinear state feedback

$$\boldsymbol{u} = \boldsymbol{G}^{-1}(\boldsymbol{x})\left(\boldsymbol{v} - \boldsymbol{F}(\boldsymbol{x})\right) \tag{19}$$

After feedback linearization processing, Eq.(5) is completely decoupled into a current subsystem and a speed subsystem. The preview controller can be designed for the linear system Eq.(18), and then the nonlinear control of the system Eq.(5) can be realized.

2.1.2 Design of the adaptive sliding mode controller

The accuracy of parameters has a significant impact on feedback linearization, but there may be modeling errors between the actual object and the theoretical model. Meanwhile, the influence of load torque disturbance is not considered in Eq.(2). These factors will bring significant linearization error and reduce control performance. Thence, an adaptive sliding mode feedback linearization method is proposed to eliminate linearization error caused by model parameter errors and disturbance of load from gear pump.

When the system Eq.(5) contains modeling error and load disturbance, the result of feedback linearization is

$$\begin{bmatrix} \dot{y}_1 \\ \ddot{y}_2 \end{bmatrix} = F(\boldsymbol{x}) + \Delta F(\boldsymbol{x}) + (\boldsymbol{G}(\boldsymbol{x}) + \Delta\boldsymbol{G}(\boldsymbol{x}))\boldsymbol{u} + D \tag{20}$$

where $\Delta F(\boldsymbol{x})$ and $\Delta\boldsymbol{G}(\boldsymbol{x})$ denote the deviations of Lie derivative caused by modeling error, and D denotes the deviation of Lie derivative caused by load disturbance T_L, shown as

$$D = \frac{B}{J^2} T_L - \frac{1}{J}\dot{T}_L \tag{21}$$

Thence, the uncertain nonlinear system is expressed as a linear system

$$\begin{cases} \dot{\boldsymbol{z}} = \boldsymbol{A}\boldsymbol{z} + \boldsymbol{B}\left(F(\boldsymbol{x}) + \Delta F(\boldsymbol{x}) + \left(\boldsymbol{G}(\boldsymbol{x}) + \Delta\boldsymbol{G}(\boldsymbol{x})\right)\boldsymbol{u} + D\right) \\ \boldsymbol{y} = \boldsymbol{C}\boldsymbol{z} \end{cases} \tag{22}$$

so the sliding mode function can be designed as

$$\boldsymbol{s}=\begin{bmatrix}s_1\\s_2\end{bmatrix}=\begin{bmatrix}e_{m1}+\alpha_1\int_0^t e_{m1}\mathrm{d}t\\ \dot{e}_{m2}+\alpha_2 e_{m2}\end{bmatrix} \tag{25}$$

The first derivative of Eq.(25) is

$$\dot{\boldsymbol{s}}=\begin{bmatrix}\dot{s}_1\\\dot{s}_2\end{bmatrix}=\begin{bmatrix}\dot{e}_{m1}+\alpha_1 e_{m1}\\ \ddot{e}_{m2}+\alpha_2\dot{e}_{m2}\end{bmatrix}=\begin{bmatrix}(\dot{y}_1-\dot{y}_{m1})+\alpha_1 e_{m1}\\ (\ddot{y}_2-\ddot{y}_{m2})+\alpha_2\dot{e}_{m2}\end{bmatrix}=$$
$$\boldsymbol{\varphi}+\Delta\boldsymbol{F}(\boldsymbol{x})+\boldsymbol{D}+(\boldsymbol{G}(\boldsymbol{x})+\Delta\boldsymbol{G}(\boldsymbol{x}))\boldsymbol{u} \tag{26}$$

where $\boldsymbol{\varphi}=\begin{bmatrix}\varphi_1\\\varphi_2\end{bmatrix}=\boldsymbol{F}(\boldsymbol{x})-\boldsymbol{v}+\begin{bmatrix}\alpha_1 e_{m1}\\\alpha_2\dot{e}_{m2}\end{bmatrix}$.

The adaptive sliding mode control law of the system can be constructed as

$$\boldsymbol{u}=-\boldsymbol{G}^{-1}(\boldsymbol{x})\left[\boldsymbol{\varphi}+\boldsymbol{k}\boldsymbol{s}+\boldsymbol{\varepsilon}\,\mathrm{sgn}(\boldsymbol{s})+\boldsymbol{\gamma}\boldsymbol{\psi}\,\mathrm{sgn}(\boldsymbol{s})\right] \tag{27}$$

where $\boldsymbol{\varepsilon}=\mathrm{diag}(\varepsilon_1,\varepsilon_2)$ and $\boldsymbol{\gamma}=\mathrm{diag}(\gamma_1,\gamma_2)$ are adaptive laws, satisfying that

$$\dot{\varepsilon}_i=k_{\varepsilon i}|s_i|,\dot{\gamma}_i=k_{\gamma i}|s_i||\varphi_i| \qquad i=1,2 \tag{28}$$

where $\boldsymbol{k}_\varepsilon$ and $\boldsymbol{k}_\gamma$ are adaptive rates. $\boldsymbol{k}=\mathrm{diag}(k_1,k_2)>0$, $\boldsymbol{\psi}=\mathrm{diag}(|\varphi_1|,|\varphi_2|)$.

The control method proposed in this paper can use $(\boldsymbol{\varepsilon},\boldsymbol{\gamma})$ to address the uncertainty and disturbance of the system, respectively, whereas the traditional SMC uses switching gain $\boldsymbol{\varepsilon}$ to address these issues, thus avoiding the problem of chattering caused by excessive switching gain.

Under the action of Eq.(27), the linearization error will gradually converge to 0, so the uncertain nonlinear system will gradually approach a linear system. In the steady state, the adaptive sliding mode feedback linearization control law will also degenerate into the traditional precise feedback linearization.

2.2 Design of preview controller

There is an assumption proposed for the system Eq.(18).

Assumption 1 The desired output $\boldsymbol{y}_d$ is a piecewise-continuously differentiable function that satisfies

$$\lim_{t\to\infty}\boldsymbol{y}_d(t)=\bar{\boldsymbol{y}}_d,\ \lim_{t\to\infty}\dot{\boldsymbol{y}}_d(t)=\boldsymbol{0} \tag{29}$$

where $\bar{\boldsymbol{y}}_d$ is a constant vector.

In addition, the desired output $\boldsymbol{y}_d$ is previewable, that is to say, at the current time t, the desired output $\boldsymbol{y}_d(\sigma)$, $t\leqslant\sigma\leqslant t+l_y$ is available, where l_y is the preview length.

Remark 1 In preview control theory, Assumption 1 is fundamental. The actual engineering studies show that the control system is only significantly affected by the recent previewable signal, whereas the desired signal outside of the previewable step has little impact. Therefore, it is generally assumed that the value outside the previewable signal is constant.

Remark 2 Examples where the expected output $\boldsymbol{y}_d$ is previewable are also common in practical applications, such as path control of robot[23], target trajectory tracking of UAV[24], position tracking of servo motor[25], etc. In the object of the electric fuel pump in this paper, when the aircraft is in the autopilot stage, it can calculate the fuel flow required for some time in the future according to the predetermined route, flight altitude and Mach number, so as to take it as predictable information.

The error vector is defined as

$$\boldsymbol{e}(t)=\boldsymbol{y}_m(t)-\boldsymbol{y}_d(t) \tag{30}$$

The new state vector is constructed as

$$\tilde{\boldsymbol{x}}(t)=\begin{bmatrix}\boldsymbol{e}(t) & \dot{\boldsymbol{z}}(t)\end{bmatrix}^{\mathrm{T}} \tag{31}$$

So system Eq.(18) can be rewritten as

$$\begin{cases}\dot{\tilde{\boldsymbol{x}}}(t)=\tilde{\boldsymbol{A}}\tilde{\boldsymbol{x}}(t)+\tilde{\boldsymbol{B}}\dot{\boldsymbol{v}}(t)-\tilde{\boldsymbol{D}}\dot{\boldsymbol{y}}_d(t)\\ \boldsymbol{e}(t)=\tilde{\boldsymbol{C}}\tilde{\boldsymbol{x}}(t)\end{cases} \tag{32}$$

where $\tilde{\boldsymbol{A}}=\begin{bmatrix}0 & \boldsymbol{C}\\0 & \boldsymbol{A}\end{bmatrix}$, $\tilde{\boldsymbol{B}}=\begin{bmatrix}0\\\boldsymbol{B}\end{bmatrix}$, $\tilde{\boldsymbol{D}}=\begin{bmatrix}\boldsymbol{I}_2\\0\end{bmatrix}$, $\tilde{\boldsymbol{C}}=\begin{bmatrix}\boldsymbol{I}_2\\0\end{bmatrix}$.

The quadratic performance index of system Eq.(32) is

$$J=\lim_{t_f\to\infty}\frac{1}{2}\int_t^{t_f}\left[\tilde{\boldsymbol{x}}^{\mathrm{T}}(\tau)\tilde{\boldsymbol{Q}}\tilde{\boldsymbol{x}}(\tau)+\dot{\boldsymbol{v}}^{\mathrm{T}}(\tau)\boldsymbol{R}\dot{\boldsymbol{v}}(\tau)\right]\mathrm{d}\tau \tag{33}$$

where $\tilde{\boldsymbol{Q}}=\mathrm{diag}(\boldsymbol{Q}_e,\boldsymbol{Q}_z)$, $\boldsymbol{Q}_e$ and $\boldsymbol{R}$ are positive definite matrices, and $\boldsymbol{Q}_z$ is a semi-positive definite matrix.

Lemma 1[26] Suppose that $(\tilde{\boldsymbol{A}},\tilde{\boldsymbol{B}})$ is stabilizable and $(\tilde{\boldsymbol{Q}}^{1/2},\tilde{\boldsymbol{A}})$ is detectable, and let $\boldsymbol{z}(t)=0$, $\boldsymbol{v}(t)=\boldsymbol{0}$, $\boldsymbol{y}_d(t)=0$ for $t<0$, the optimal control input of the system Eq.(18) is

$$\boldsymbol{v}(t)=-\boldsymbol{k}_e\int_0^t\boldsymbol{e}(\sigma)\mathrm{d}\sigma-\boldsymbol{k}_z\boldsymbol{z}(t)+\boldsymbol{f}(t) \tag{34}$$

where $\boldsymbol{k}_e$ and $\boldsymbol{k}_z$ are the feedback gain matrices, shown as

$$\boldsymbol{k}_e=\boldsymbol{R}^{-1}\tilde{\boldsymbol{B}}^{\mathrm{T}}\tilde{\boldsymbol{P}}_e,\ \boldsymbol{k}_z=\boldsymbol{R}^{-1}\tilde{\boldsymbol{B}}^{\mathrm{T}}\tilde{\boldsymbol{P}}_z \tag{35}$$

$$\boldsymbol{f}(t)=\boldsymbol{R}^{-1}\tilde{\boldsymbol{B}}^{\mathrm{T}}\int_0^{l_y}\exp(\sigma\boldsymbol{A}_{\mathrm{c}}^{\mathrm{T}})\tilde{\boldsymbol{P}}\tilde{\boldsymbol{D}}\boldsymbol{y}_{\mathrm{d}}(t+\sigma)\mathrm{d}\sigma\ ,$$

$\tilde{\boldsymbol{A}}_{\mathrm{c}}=\tilde{\boldsymbol{A}}-\tilde{\boldsymbol{B}}\boldsymbol{R}^{-1}\tilde{\boldsymbol{B}}^{\mathrm{T}}\tilde{\boldsymbol{P}}$ is an asymptotically stable matrix. $\tilde{\boldsymbol{P}}=[\tilde{\boldsymbol{P}}_e\quad\tilde{\boldsymbol{P}}_z]$ is the only positive semi-definite solution that satisfies the Riccati equation

$$\tilde{\boldsymbol{A}}^{\mathrm{T}}\tilde{\boldsymbol{P}}+\tilde{\boldsymbol{P}}\tilde{\boldsymbol{A}}-\tilde{\boldsymbol{P}}\tilde{\boldsymbol{B}}\boldsymbol{R}^{-1}\tilde{\boldsymbol{B}}^{\mathrm{T}}\tilde{\boldsymbol{P}}+\tilde{\boldsymbol{Q}}=0 \tag{36}$$

According to Eq.(34), the controller is composed of three parts. The first of them is the integral effect of tracking error, followed by state feedback, and the last is the preview control effect using the desired output of future information.

The control structure block diagram of the system is shown in Fig.1, which can be divided into three parts. The controller is composed of a preview controller and an adaptive sliding mode feedback linearization controller. The PMSM adopts the vector control method with $i_d=0$, the driving system is powered by a 270 V high voltage DC bus, the PMSM is coaxially connected with the gear pump, and the gear pump is considered as the load of the motor. It is worth noting that in actual engineering applications, the flowmeter accuracy is insufficient to accurately depict the magnitude of the gear pump's flow pulsation, so a low-pass filter is utilized to simulate the flowmeter.

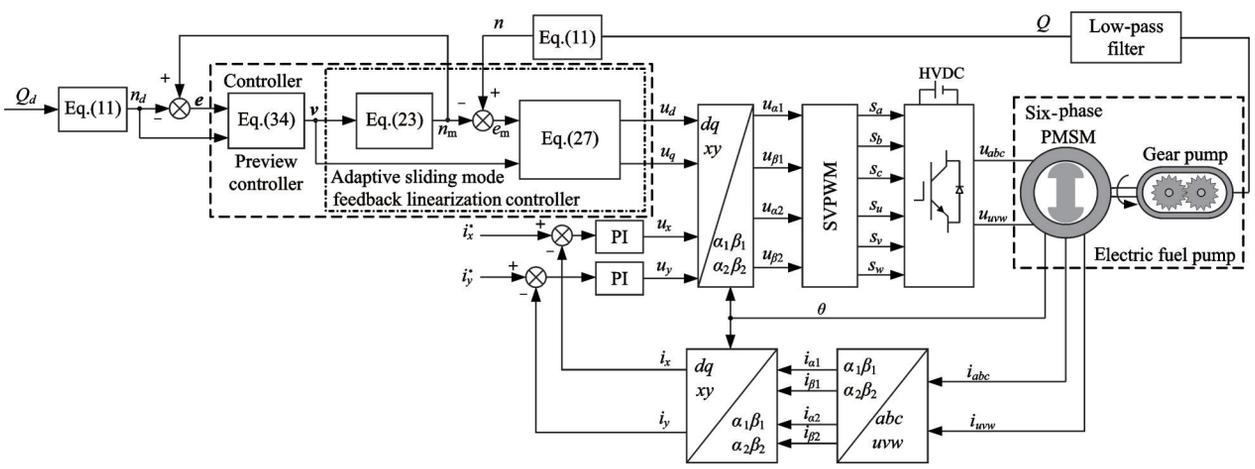

Fig.1 Block diagram of electric fuel pump preview control system based on adaptive feedback linearization

2.3 Stability analysis

2.3.1 Stability of the adaptive sliding mode controller

Assumption 2 The distribution function matrix $\boldsymbol{G}(\boldsymbol{x})$ of the system Eq.(15) is invertible.

Let

$$\hat{\boldsymbol{G}}(\boldsymbol{x})=\Delta\boldsymbol{G}(\boldsymbol{x})\boldsymbol{G}^{-1}(\boldsymbol{x})=\left[\hat{\boldsymbol{G}}_1(\boldsymbol{x})\quad\hat{\boldsymbol{G}}_2(\boldsymbol{x})\right] \tag{37}$$

where $\hat{\boldsymbol{G}}_i(\boldsymbol{x})$ is the ith column of $\hat{\boldsymbol{G}}(\boldsymbol{x})$, denoted as

$$\hat{\boldsymbol{G}}_i(\boldsymbol{x})=[G_{1i}\quad G_{2i}]^{\mathrm{T}}\quad i=1,2 \tag{38}$$

Assumption 3 The uncertain matrices $\Delta\boldsymbol{F}(\boldsymbol{x})$, $\Delta\boldsymbol{G}(\boldsymbol{x})$ and D of the system Eq.(20) are bounded, satisfying

$$\begin{cases}\left\|\Delta F_i(\boldsymbol{x})+D_i\right\|<a_i\\ \max_j\left(\left|\hat{G}_{ij}(\boldsymbol{x})\right|\right)<b_i\quad 0<b_i<\dfrac{1}{2};i=1,2\\ \left|\hat{G}_{ii}(\boldsymbol{x})\right|<c_i<1\qquad\qquad c_i>0\end{cases} \tag{39}$$

where $\Delta F_i(\boldsymbol{x})$ and D_i are the ith row of the matrix $\Delta\boldsymbol{F}(\boldsymbol{x})$ and D; and a_i, b_i and c_i the corresponding upper bounds, respectively. $\hat{G}_{ij}(\boldsymbol{x})$ is the element of the ith row and jth column of the matrix $\hat{\boldsymbol{G}}(\boldsymbol{x})$; and $\hat{G}_{ii}(\boldsymbol{x})$ the diagonal element of the matrix $\hat{\boldsymbol{G}}(\boldsymbol{x})$.

Remark 3 The external load does not suddenly change in the voltage control loop with a short sampling interval. Therefore, in each fixed sampling interval, we can assume that the load torque T_{L} generated by the gear pump is constant, and its derivative $\dot{T}_{\mathrm{L}}$ is equal to zero. Obviously, D is bounded.

Theorem 1 The system Eq.(22) will converge asymptotically under the action of the adaptive sliding mode control law shown in Eq.(27).

Proof Parameter errors are defined as

$$\begin{cases}\tilde{\varepsilon}_i=\varepsilon_i-\varepsilon_{i0}\\ \tilde{\gamma}_i=\gamma_i-\gamma_{i0}\end{cases}\quad i=1,2 \tag{40}$$

where

$$\begin{cases}\varepsilon_{i0}=a_i/(1-c_i)\\ \gamma_{i0}=2b_i/(1-c_i)\end{cases} \tag{41}$$

The Lyapunov function is defined as

$$V=\frac{1}{2}\sum_{i=1}^{2}s_i^2+\frac{1}{2}\sum_{i=1}^{2}\frac{1-c_i}{k_{\varepsilon i}}\tilde{\varepsilon}_i^2+\frac{1}{2}\sum_{i=1}^{2}\frac{1-c_i}{k_{\gamma i}}\tilde{\gamma}_i^2 \tag{42}$$

The first derivative of Eq.(42) is

$$\dot{V}=\sum_{i=1}^{2}\left(s_i\dot{s}_i+\frac{1-c_i}{k_{\varepsilon i}}\dot{\tilde{\varepsilon}}_i\tilde{\varepsilon}_i+\frac{1-c_i}{k_{\gamma i}}\dot{\tilde{\gamma}}_i\tilde{\gamma}_i\right)=\sum_{i=1}^{2}v_i \tag{43}$$

According to Assumption 2 and Eqs.(26, 28, 40), it can be concluded that

$$\begin{aligned}v_i=&s_i\dot{s}_i+\frac{1-c_i}{k_{\varepsilon i}}\dot{\tilde{\varepsilon}}_i\tilde{\varepsilon}_i+\frac{1-c_i}{k_{\gamma i}}\dot{\tilde{\gamma}}_i\tilde{\gamma}_i=\\ &\left(\left(\Delta F_i(\boldsymbol{x})+D_i\right)-\sum_{j=1}^{2}\hat{G}_{ij}(\boldsymbol{x})\varphi_j\right)s_i-\\ &k_i\left(1+\hat{G}_{ii}(\boldsymbol{x})\right)|s_i|-\left(\left(1+\hat{G}_{ii}(\boldsymbol{x})\right)\varepsilon_i+\right.\\ &\left.\left(1+\hat{G}_{ii}(\boldsymbol{x})\right)\gamma_i|\psi_i|\right)|s_i|+(1-c_i)(\varepsilon_i-\varepsilon_{i0})|s_i|+\\ &(1-c_i)\left(\gamma_i-\gamma_{i0}\right)|s_i||\varphi_i|\end{aligned} \tag{44}$$

According to Assumption 3 and Eq.(41), we can get

$$\begin{aligned}v_i<&\left(a_i+2b_i|\psi_i|\right)|s_i|-k_i(1-c_i)|s_i|-\\ &\left((1-c_i)\varepsilon_i+(1-c_i)\gamma_i|\psi_i|\right)|s_i|+\\ &(1-c_i)(\varepsilon_i-\varepsilon_{i0})|s_i|+(1-c_i)\left(\gamma_i-\gamma_{i0}\right)\cdot\\ &|s_i||\psi_i|=-k_i(1-c_i)|s_i|+a_i|s_i|-(1-c_i)\cdot\\ &\varepsilon_i|s_i|+(1-c_i)(\varepsilon_i-\varepsilon_{i0})|s_i|+2b_i|s_i||\psi_i|-\\ &(1-c_i)\gamma_i|s_i||\psi_i|+(1-c_i)\left(\gamma_i-\gamma_{i0}\right)|s_i||\psi_i|=\\ &-k_i(1-c_i)|s_i|<0\end{aligned} \tag{45}$$

Therefore, $\dot{V}<0$, the tracking error of the controller will gradually converge to 0.

2.3.2 Stability of the closed-loop system

Lemma 2[23] Suppose that $\left(\tilde{A},\tilde{B}\right)$ is stabilizable and $\left(\tilde{Q}^{1/2},\tilde{A}\right)$ is detectable, the optimal control input of system Eq.(32) under performance index function Eq.(33) is

$$\dot{\boldsymbol{v}}(t)=-\boldsymbol{R}^{-1}\tilde{\boldsymbol{B}}^{\mathrm{T}}\tilde{\boldsymbol{P}}\tilde{\boldsymbol{x}}(t)-\boldsymbol{R}^{-1}\tilde{\boldsymbol{B}}^{\mathrm{T}}\boldsymbol{g}(t) \tag{46}$$

where $\boldsymbol{g}(t)=-\int_0^{l_y}\exp\left(\sigma\tilde{\boldsymbol{A}}_c^{\mathrm{T}}\right)\tilde{\boldsymbol{P}}\tilde{\boldsymbol{D}}\dot{\boldsymbol{y}}_{\mathrm{d}}(t+\sigma)\mathrm{d}\sigma$.

Theorem 2 If the desired output $\boldsymbol{y}_{\mathrm{d}}$ satisfies Assumption 1, the closed-loop system Eq.(32) realizes complete regulation, namely

$$\lim_{t\to\infty}\boldsymbol{e}(t)=\boldsymbol{0} \tag{47}$$

and

$$\lim_{t\to\infty}\tilde{\boldsymbol{x}}(t)=\bar{\tilde{\boldsymbol{x}}},\ \lim_{t\to\infty}\boldsymbol{v}(t)=\bar{\boldsymbol{v}} \tag{48}$$

where $\bar{\tilde{\boldsymbol{x}}}$ and $\bar{\boldsymbol{v}}$ are constant vectors that satisfy

$$\begin{cases}\boldsymbol{0}=\boldsymbol{A}\bar{\tilde{\boldsymbol{x}}}+\boldsymbol{B}\bar{\boldsymbol{v}}\\ \bar{\boldsymbol{y}}_{\mathrm{d}}=\boldsymbol{C}\bar{\tilde{\boldsymbol{x}}}\end{cases} \tag{49}$$

Proof Denote

$$\boldsymbol{\theta}(t)=-\tilde{\boldsymbol{B}}\boldsymbol{R}^{-1}\tilde{\boldsymbol{B}}^{\mathrm{T}}\boldsymbol{g}(t)-\boldsymbol{D}\dot{\boldsymbol{y}}_{\mathrm{d}}(t)$$

According to Lemma 2, the closed-loop system (32) can be expressed as

$$\dot{\tilde{\boldsymbol{x}}}(t)=\tilde{\boldsymbol{A}}_{\mathrm{c}}\tilde{\boldsymbol{x}}(t)+\boldsymbol{\theta}(t) \tag{50}$$

Hence

$$\tilde{\boldsymbol{x}}(t)=e^{\tilde{\boldsymbol{A}}_{\mathrm{c}}(t-t_0)}\tilde{\boldsymbol{x}}(t_0)+\int_{t_0}^{t}e^{\tilde{\boldsymbol{A}}_{\mathrm{c}}(t-\tau)}\boldsymbol{\theta}(\tau)\mathrm{d}\tau \tag{51}$$

Under Assumption 1, we can get that $\lim_{t\to\infty}\dot{\boldsymbol{y}}_{\mathrm{d}}(t)=0$. Based on the expression of $\boldsymbol{g}(t)$, it is evident that $\dot{\boldsymbol{y}}_{\mathrm{d}}$ is taken from time t, so $\lim_{t\to\infty}\boldsymbol{g}(t)=\boldsymbol{0}$, then $\lim_{t\to\infty}\boldsymbol{\theta}(t)=\boldsymbol{0}$. The following only needs to prove that $\lim_{t\to\infty}\tilde{\boldsymbol{x}}(t)=0$.

Since $\tilde{\boldsymbol{A}}_{\mathrm{c}}$ is asymptotically stable, there are constants $m\geqslant 0$ and $n\geqslant 0$ such that

$$\left\|e^{\tilde{\boldsymbol{A}}_{\mathrm{c}}(t-t_0)}\tilde{\boldsymbol{x}}(t_0)\right\|\leqslant me^{-n(t-t_0)}\left\|\tilde{\boldsymbol{x}}(t_0)\right\| \tag{52}$$

By normalizing Eq.(51), we can get

$$\left\|\tilde{\boldsymbol{x}}(t)\right\|\leqslant me^{-n(t-t_0)}\left\|\tilde{\boldsymbol{x}}(t_0)\right\|+\int_{t_0}^{t}me^{-n(t-\tau)}\left\|\boldsymbol{\theta}(\tau)\right\|\mathrm{d}\tau \tag{53}$$

where $\lim_{t\to\infty}me^{-n(t-t_0)}\left\|\tilde{\boldsymbol{x}}(t_0)\right\|=0$.

According to the L'Hospital's rule

$$\lim_{t\to\infty}\int_{t_0}^{t}me^{-n(t-\tau)}\left\|\boldsymbol{\theta}(\tau)\right\|\mathrm{d}\tau=\lim_{t\to\infty}\frac{\int_{t_0}^{t}me^{n\tau}\left\|\boldsymbol{\theta}(\tau)\right\|\mathrm{d}\tau}{e^{nt}}=$$

$$\lim_{t\to\infty}\frac{me^{nt}\left\|\boldsymbol{\theta}(t)\right\|}{ne^{nt}}=\frac{m}{n}\lim_{t\to\infty}\left\|\boldsymbol{\theta}(t)\right\|=0 \tag{54}$$

We can get $\lim_{t\to\infty}\tilde{\boldsymbol{x}}(t)=\boldsymbol{0}$, then $\lim_{t\to\infty}\boldsymbol{e}(t)=0$.

3 Simulation Results and Discussion

The proposed control method is contrasted with PI control and traditional SMC to confirm its effectiveness.

The error vector of the traditional SMC is defined as

$$\boldsymbol{e}=\begin{bmatrix}e_1\\e_2\end{bmatrix}=\begin{bmatrix}y_{d1}-y_1\\y_{d2}-y_2\end{bmatrix}$$

and the sliding mode switching function is constructed as

$$\boldsymbol{s}=\begin{bmatrix}s_1\\s_2\end{bmatrix}=\begin{bmatrix}e_1+\beta_1\int_0^t e_1\mathrm{d}t\\ \dot{e}_2+\beta_2 e_2\end{bmatrix}$$

then the sliding mode control law can be developed

$$\boldsymbol{v}=\begin{bmatrix}v_1\\v_2\end{bmatrix}=\begin{bmatrix}\dot{y}_{d1}+\beta_1 e_1+\rho_1 s_1+\eta_1\,\mathrm{sgn}(s_1)\\ \ddot{y}_{d2}+\beta_2\dot{e}_2+\rho_2 s_2+\eta_2\,\mathrm{sgn}(s_2)\end{bmatrix}$$

$$\boldsymbol{u}=\boldsymbol{G}^{-1}(\boldsymbol{x})\left[\boldsymbol{v}-\boldsymbol{F}(\boldsymbol{x})\right]$$

In MATLAB/Simulink, the simulation model of electric fuel pump system is built. Table 1 shows the parameters of the six-phase PMSM, and the properties of the gear pump are detailed in Table 2.

Table 1 Parameters of the six-phase PMSM

Parameter	Value
Rated speed/(r•min^{-1})	6 000
Number of pole-pairs	4
Stator resistance/Ω	0.5
Stator inductance/mH	1.2
Flux linkage/Wb	0.05
Rotational inertia/(kg•m^2)	0.000 84
Damping coefficient/(N•m•s)	0.000 02

Table 2 Parameters of the gear pump

Parameter	Value
Tooth number	14
Module	2.5
Tooth width/mm	18
Center-distance/mm	36
Rated speed/(r•min^{-1})	6 000
Rated flow/(L•min^{-1})	56
Inlet pressure/MPa	0.3
Outlet pressure/MPa	8

In addition, the gear pump throttling coefficient $C_d=0.7$, fuel density $\rho=780$ kg/m^3, tank pressure $P_t=0.1$ MPa. According to the flow of gear pump under rated condition, the equivalent throttling orifice area $A_t=1.051$ mm^2 and the oil outlet area $A_o=9.368$ mm^2 are calculated.

The parameter setting of the preview controller based on adaptive sliding mode control (PASMC) are $\boldsymbol{Q}_e=\mathrm{diag}(7\times10^6,0)$, $\boldsymbol{Q}_z=\mathrm{diag}(1.5\times10^4,1,0)$, $\boldsymbol{R}=\mathrm{diag}(2\times10^{-5},0)$, preview length $l_y=2$ ms; $\boldsymbol{\alpha}=[50,80]$, $\boldsymbol{k}=[10,30]$, $\boldsymbol{k}_\varepsilon=[1,10]$, $\boldsymbol{k}_\gamma=[2,1]$. The parameters setting of sliding mode controller are $\boldsymbol{\beta}=[50,80]$, $\boldsymbol{\rho}=[10,30]$, $\boldsymbol{\eta}=[1.2\times10^5,5\times10^7]$. The parameters setting of PI controller are $\boldsymbol{k}_\mathrm{P}=[0.01,0.05]$, $\boldsymbol{k}_\mathrm{I}=[5,0.8]$. In addition, in order to better satisfy Assumption 1, the desired output flow is processed by a first-order inertial loop

$$G(s)=\frac{1}{Ts+1}$$

where T is the time constant, and it is taken as 0.01.

Case 1 Constantly desired flow output

The desired flow is set to 35 L/min, and Fig.2 depicts the system flow response.

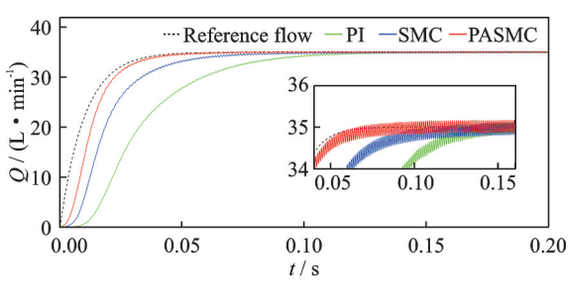

Fig.2 Flow response of the system for Case 1

As can be observed, the PASMC responds more quickly than the PI and SMC due to the use of preview control, and there is no overshoot.

The changes of the d-axis and the q-axis current of the motor are shown in Fig.3. Compared with SMC, the error of i_d obtained using PASMC is significantly smaller. Affected by the pulsating torque of the gear pump, i_q changes periodically. The enlarged view shows that the fluctuation of i_q

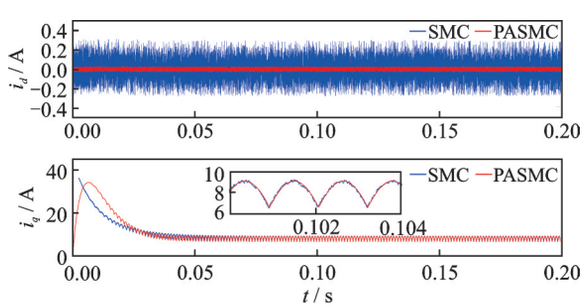

Fig.3 Comparison of current i_d and i_q

under the PASMC is smaller than the SMC.

In addition, the change of the sliding surfaces is shown in Fig.4. In the process of modeling the six-phase PMSM, the load disturbance is not considered, and the switching term of SMC is directly utilized to overcome the effect of the load torque. For the traditional SMC, only a larger sliding mode gain can be used to overcome the influence of the load torque, which causes the problem of chattering. With a smaller sliding mode switching gain, the PASMC method described in this study may change the control law in accordance with the output of the reference model and the output of the actual object, avoiding the impact of load disturbance. In comparison to the SMC, the proposed PASMC chattering is significantly less at steady state, as seen in Fig.4.

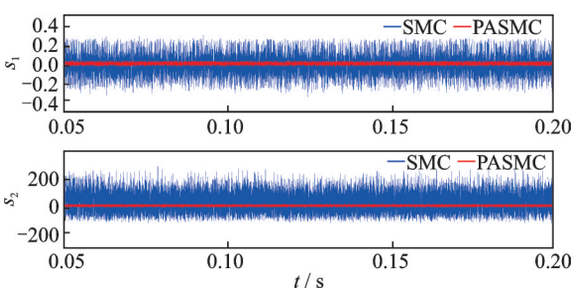

Fig.4 Comparison of sliding surfaces s_1 and s_2

Under the condition that the desired output flow is constant, different preview lengths l_y are selected to verify the influence of different preview lengths on the system control effect. $l_y = 0$ ms means that the system does not adopt preview control.

Fig.5 shows the simulation results. It is obvious that the system response time has been markedly shortened due to the inclusion of preview control. It is significant to mention that with the constant rise in preview length, the acceleration rate of the system response speed slows down significantly. This is consistent with the actual situation, that is to say, the farther the future information is from the current moment, the less the impact on the state of the system at the current moment.

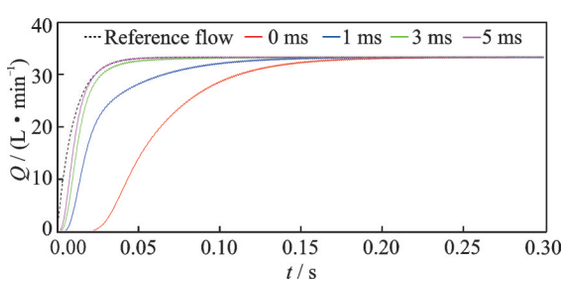

Fig.5 Flow response of the system under different preview lengths

Case 2 Considering the existence of modeling error

To verify the robustness of the PASMC, parameter uncertainties of +10% and −10% are considered respectively. Moreover, in a high-temperature and high-pressure environment such as aero-engine, the permanent magnets in the PMSM may be irreversibly demagnetized due to high temperature, which will seriously reduce the performance of the permanent magnet and lead to the reduction of the torque performance of the motor, so in Case 2.2 a larger flux linkage error is considered.

Case 2.1 $\Delta R = 10\% R$, $\Delta L = 10\% L$, $\Delta J = 10\% J$, $\Delta B = 10\% B$, $\Delta \psi_f = 10\% \psi_f$

Case 2.2 $\Delta R = -10\% R$, $\Delta L = -10\% L$, $\Delta J = -10\% J$, $\Delta B = -10\% B$, $\Delta \psi_f = -0.03$ Wb

Fig.6 and Fig.7 show the fuel flow response when modeling errors exist. It can be seen that the PASMC can achieve rapid response with minimal steady-state errors. The traditional PI control has a large overshoot, at the same time, considering that high temperature may cause large flux linkage er-

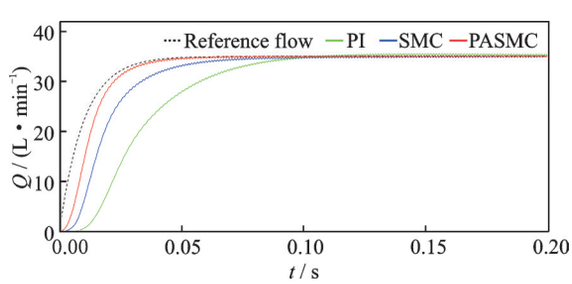

Fig.6 Flow response of the system for Case 2.1

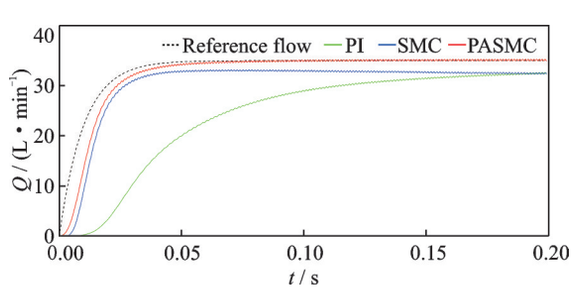

Fig.7 Flow response of the system for Case 2.2

ror, PI and SMC have large steady-state errors. These outcomes confirmed that the PASMC is highly robust to the model's uncertainty.

Case 3 Considering a wide range of flow changes

To verify the flow regulation ability of the novel control approach, it is configured to change the desired flow from 20 L/min to 56 L/min.

As shown in Fig.8, the PASMC has a faster response speed compared with the PI and the SMC, indicating that the system's response time to fuel commands can be sped up through preview control. Especially in the case of large flow, the SMC has a large steady-state error, indicating that the existing sliding mode switching gain can no longer overcome the influence of the load torque.

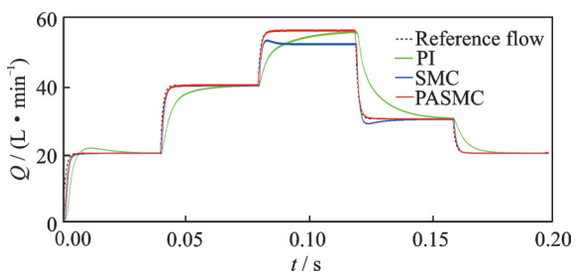

Fig.8 Flow response of the system for Case 3

Table 3 shows the comparison of the rise time and absolute relative tracking error of the three methods. In comparison to the PI control, the response speed of SMC and PASMC is significantly faster, but the SMC has a large steady-state error. The results demonstrated that under a wide range of flow changes, the method described in this work performs better in terms of regulation and tracking.

Table 3 Tracking error of three control methods

Parameter	PI	SMC	PASMC
Mean rise time/s	0.090	0.023	0.020
Maximum absolute relative tracking error/%	1.231	7.482	0.567
Mean absolute relative tracking error/%	0.890	2.130	0.439

4 Conclusions

To improve the robustness of the aviation electric fuel pump flow control system and the speed of response to fuel command, this work proposes a design approach for a preview controller based on adaptive sliding mode feedback linearization, resulting in the conclusions that are listed below.

(1) The feedback linearization technique is utilized to completely decouple the electric fuel pump into linear subsystems, which helps to ease the design of the preview controller and accelerates the system response to fuel command.

(2) An adaptive sliding mode control method is explored to separate the uncertainty caused by modeling error and load disturbance, which significantly weakens the chattering problem of sliding mode control. In addition, the adaptive control does not require accurate uncertain boundary information, which enhances the control performance.

(3) As demonstrated by the simulation results, even when load disturbance and modeling error are existent, the preview control method still exhibits excellent robustness, quick response, and small steady-state error.

It is worth mentioning that this paper lacks actual experiments. For one thing, this paper uses classical methods for modeling, which have been proven to reflect the actual situation. For another, the experiment requires high safety, and the laboratory lacks the conditions for high-voltage experiments at present. Moreover, the gear pump has different flow characteristics in the instance of high and low flow rate. In future research of actual engineering, more accurate flow characteristics of the gear pump should be explored, so as to obtain better control performance.

References

[1] SARLIOGLU B, MORRIS C T. More electric aircraft: Review, challenges, and opportunities for commercial transport aircraft[J]. IEEE Transactions on Transportation Electrification, 2015,1(1): 54-64.

[2] RENDON M A, SANCHEZ R C D, GALLO M J, et al. Aircraft hybrid-electric propulsion: Development trends, challenges, and opportunities[J]. Journal of Control, Automation and Electrical Systems, 2021,32(5): 1244-1268.

[3] YU L, ZHANG Z R, ZHANG J, et al. Study and im-

plementation on high-speed starter/generator for more electric engine application[J]. Chinese Journal of Electrical Engineering, 2020,40(14): 4615-4628.

[4] SONG J Q, PAN M X, HUNG J Q. Technical analysis and system scheme for aeroengine distributed control system[J]. Journal of Aerospace Power, 2013, 28(10): 2391-2400.

[5] MORIOKA N, OYORI H. Fuel pump system configuration for the more electric engine[C]//Proceedings of Aerospace Technology Conference and Exposition. [S.l.]: SAE, 2011.

[6] MORIOKA N, OYORI H, GONDA Y, et al. Development of the electric fuel system for the more electric engine[C]//Proceedings of ASME Turbo Expo 2014: Turbine Technical Conference and Exposition. Düsseldorf, Germany: [s.n.], 2014.

[7] DING R Z, XIAO L F, JIN X. Robust control for electric fuel pump with variant nonlinear loads based on a new combined sliding mode surface[J]. International Journal of Control, Automation, and Systems, 2019,17(3): 716-728.

[8] TROCHELMANN N, STUMP P B, THIELECKE F, et al. A robust pressure controller for a variable speed AC motor pump-application to aircraft hydraulic power packsges[C]//Proceedings of the BATH/ASME 2018 Symposium on Fluid Power and Motion Control. Bath, UK: [s.n.], 2018.

[9] SHERIDAN T B. Three models of preview control[J]. IEEE Transactions on Human Factors in Electronics, 1966, HFE-7(2): 91-102.

[10] CAO R, LU Y, ZHEN Z. Tracking control of transition window for aerospace vehicles based on robust preview control[J]. Aerospace Science and Technology, 2021,114: 106748.

[11] CHENG Jianfeng, DONG Xinmin, XUE Jianping, et al. Fuzzy preview controller design for aircraft-pilot closed loop system[J]. Acta Aeronautica et Astronautica Sinica, 2014,35(3): 807-820.(in Chinese)

[12] UCHIDA D, SHIMOMURA T, HAMADA Y. Aircraft gust alleviation preview control with a discrete-time LPV model in consideration of the elastic mode[J]. IFAC-PapersOnLine, 2019,52(28): 184-189.

[13] BHATIA A K, JIANG J, KUMAR A, et al. Adaptive preview control with deck motion compensation for autonomous carrier landing of an aircraft[J]. International Journal of Adaptive Control and Signal Processing, 2021,35(5): 769-785.

[14] MA H F, LI Y M. A novel dead zone reaching law of discrete-time sliding mode control with disturbance compensation[J]. IEEE Transactions on Industrial Electronics, 2020,67(6): 4815-4825.

[15] DU H B, YU X H, CHEN M Z Q, et al. Chattering-free discrete-time sliding mode control[J]. Automatica, 2016, 68: 87-91.

[16] WANG P C, ZHANG D F, LU B C. Robust fuzzy sliding mode control based on low pass filter for the welding robot with dynamic uncertainty[J]. Industrial Robot: The international Journal of Robotics Research and Application, 2019,47(1): 111-120.

[17] JIA T, LI X Z, ZHANG X Y. Neural network sliding mode control for vehicle inertial stabilized platform[J]. Control Theory & Applications, 2021, 38(1): 13-22.

[18] YUAN Lei. Control principle and MATLAB simulation of modern permanent magnet synchronous motor [M]. Beijing: Beihang University Press, 2016: 202-204.(in Chinese)

[19] XU Xianliang, ZHAO Lianchun, WANG Chuanli. Compound gear pump [M]. Beijing: China Machine Press, 2006: 4-8.(in Chinese)

[20] LI Zhongjie. Characteristic analysis and experimental study of aviation electric fuel pump[D]. Nanjing: University of Nanjing Aeronautics and Astronautics, 2020.(in Chinese)

[21] LI Y L, LIU K, WANG X J. Dynamic reappearance on torque calculation in a gear pump with external Mesh[J]. Transactions of the Chinese Society of Agricultural Machinery, 2006(3): 142-144.

[22] ZHANG K, WANG L M. Adaptive dynamic sliding mode control of permanent magnet linear synchronous motor based on feedback linearization[J]. Transactions of China Electrotechnical Society, 2021,36(9): 4016-4024.

[23] RUSCELLI F, LAURENZI A, HOFFMAN E M, et al. Omnidirectional walking pattern generator combining virtual constraints and preview control for humanoid robots[J]. Frontiers in Robotics and AI, 2021, 8: 660004.

[24] ZHEN Z Y, JIANG S Y, MA K. Automatic carrier landing control for unmanned aerial vehicles based on preview control and particle filtering[J]. Aerospace Science and Technology, 2018, 81(10): 99-107.

[25] LAN Y H, HE J L, LI P, et al. Optimal preview repetitive control with application to permanent magnet synchronous motor drive system[J]. Journal of the Franklin Institute, 2020, 357(15): 10194-10210.

[26] LIAO F C, TANG Y Y, LIU H P, et al. Design of an optimal preview controller for continuous-time systems[J]. International Journal of Wavelets, Multiresolu-

tion and Information Processing, 2011,9(4): 655-673.

Acknowledgements This work was supported by the National Natural Science Foundation of China (No.51876089), the Postgraduate Research & Practice Innovation Program of Nanjing University of Aeronautics and Astronautics (No. xcxjh20210204), and the Open Foundation of the State Key Laboratory of Fluid Power and Mechatronic Systems (No. GZKF-202005).

Authors Mr. **MENG Xiangshuo** is a postgraduate currently at College of Energy and Power Engineering, Nanjing University of Aeronautics and Astronautics. His major is power machinery and engineering and his research interest is sliding mode control and fault-tolerant control for mechanical and electrical systems.

Dr. **XIAO Lingfei** currently holds the position of associate professor within the Jiangsu Province Key Laboratory of Aerospace Power Systems, Nanjing University of Aeronautics and Astronautics. She received her Ph.D. degree from Zhejiang University in 2008. Her main research interest lies in advanced control theory and application in complex mechanical and electrical systems, and aircraft engine systems.

Author contributions Mr. **MENG Xiangshuo** designed the study, compiled the models, conducted the analysis, interpreted the results, and wrote the manuscript. Dr. **XIAO Lingfei** contributed to the discussion and background of the study. Mr. **MA Leiming** contributed data and model components for the electric fuel pump model. All authors commented on the manuscript draft and approved the submission.

Competing interests The authors declare no competing interests.

(Production Editor: SUN Jing)

基于自适应滑模反馈线性化的航空电动燃油泵预见控制器设计

孟祥硕[1], 肖玲斐[1,2], 马磊明[3]

(1.南京航空航天大学能源与动力学院,南京 210016,中国; 2.浙江大学流体动力与机电系统国家重点实验室,杭州 310027,中国; 3.南京航空航天大学自动化学院,南京 211106,中国)

摘要:以六相永磁同步电机直接驱动外啮合齿轮泵的航空电动燃油泵为对象,研究了其流量系统的控制器设计问题,提出了一种基于自适应滑模反馈线性化的预见控制器设计方法。首先,建立六相永磁同步电动机和外啮合齿轮泵的数学模型。其次,利用反馈线性化方法处理电动燃油泵这一非线性化模型,方便后续预见控制器的设计;接着,采用自适应滑模控制方法消除了由模型不确定性引起的反馈线性化误差,该方法可以将建模误差和负载扰动带来的不确定性分开处理,从而避免较大的切换增益引起抖振,同时不需要精确的不确定性的边界信息,从而提高了控制性能。最后,在反馈线性化得到线性模型上设计预见流量控制器,加快控制系统对燃油指令的响应速度。仿真结果表明,该控制方案具有较快的响应速度、较强的鲁棒性能和优良的抑制抖振能力。

关键词:航空电动燃油泵;预见控制;自适应滑模控制;反馈线性化;建模不确定性